Geophys. J. Int. (1996) **124,** 304–314

On the effect of diffraction on traveltime measurements

'Oli Gudmundsson
Research School of Earth Sciences, Australian National University, Canberra, ACT 0200, *Australia*

Accepted 1995 August 16. Received 1995 August 1; in original form 1995 April 1

SUMMARY

All observed waves are of finite frequency and are sensitive to a finite volume of the medium through which they pass. Diffraction causes a loss of information about time contained in the initial front of a wavefield (often referred to as wavefront healing). This effect depends upon frequency and propagation distance and imposes a low-pass filter on the spatial resolution of time measurements. A sequence of canonical, numerical experiments that simulate the diffraction of a perturbed plane wave at a fixed distance is described. Traveltimes are measured using a variety of techniques on a range of waveforms. It is empirically verified that a single Fresnel zone describes the spatial filtering effect of the propagation of a broad-band wavefield, even in the regime where the initial time perturbation cannot be represented by a linear perturbation term. For narrow-band wavefields, more Fresnel zones come into play as the bandwidth is reduced. Measurements of time include a component of signal-generated noise coherent over a small scale which scales with the Fresnel zone. It is found that, for traveltimes measured by automated picking, the width of the Fresnel zone is described by a time delay of $|\delta t| < T/4$ (here T is one period). On the other hand, the width of the Fresnel zone for traveltimes measured by correlation is wider, characterized by a time delay of $|\delta t| < T/4$.

Key words: diffraction, traveltime, wave propagation.

INTRODUCTION

Ray theory forms the basis for interpreting traveltime, or phase, observations in seismology. At the same time, the difficulties in interpreting traveltimes measured from finite-frequency seismograms have been known for some time (Claerbout 1976). With the advent of 3-D inversion (tomography) in seismology, based on traveltimes or surface-wave dispersion, the limitations of ray theory have become an increasing worry. Wielandt (1987), Petersen (1990) and other Soviet authors (see Petersen 1990) pointed out that diffraction and scattering can cause a systematic bias in velocity estimates. Energy that travels along a fast path is more likely to affect a traveltime reading than energy that propagates along a slow path because it arrives earlier. Therefore, the average wave speed appears higher than the volumetric mean of the intrinsic wave speed. Nolet & Moser (1993) and Roth, Muller & Snieder (1993) have shown that a modest level of heterogeneity in the Earth's mantle can render this effect significant for teleseismic body waves. This is a ray-theoretical effect caused by the neglect of the second-order time perturbation due to ray bending (Sambridge & Snieder 1993). A similar effect arises from diffraction associated with smoothing of time perturbations in the initial wavefront. The same holds for lateral variations in the wavefront of a surface wave.

When a wavefront passes through a heterogeneous structure it acquires complexity. In particular, perturbations of time are introduced by local variations in wave speed. As the perturbed wavefront advances to a remote recorder, its complexity evolves. Advanced portions of the wavefront expand in space and to some degree mask the delayed portions by a process often referred to as wavefront healing (Claerbout 1985). Inherent in this process is a loss of time information that is frequency-dependent. Wavefront healing is a geometrical diffraction effect, and simple geometrical arguments, or mathematical analysis, lead one to estimate its importance or to scale it by the Fresnel zone.

This argument is demonstrated in Fig. 1. A plane wave (dashed) is perturbed in phase (solid curve). The wavefront proceeds to propagate a distance, L, to a receiver at point **R** through a homogeneous medium of velocity, v. Energy at point **P** arrives at the receiver at **R** at time t_0 having followed a straight path. Energy from adjacent parts of the wavefront arrives slightly later. All energy within the distance $x_F/2$, measured on the wavefront from **P**, arrives within some time delay, δt, of the minimum-time arrival. If we choose this time delay as a quarter of the period of the recorded wave, $T/4$, all this energy interferes constructively. We can then say that the wavefield recorded at **R** represents an integral of the wavefield around **P** and that variations in phase on the wavefront around

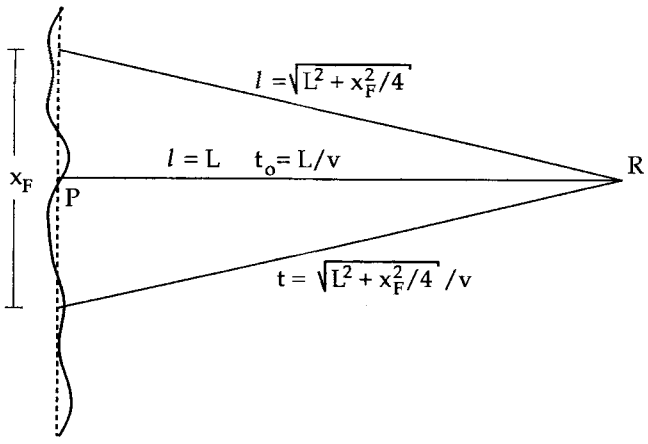

$$\delta t = t - t_o = \left[\sqrt{L^2 + x_F^2/4} - L\right]/v = T/4 \Rightarrow$$

$$x_F = \sqrt{2vTL + v^2T^2/4} = \sqrt{2\lambda L + \lambda^2/4}$$

Figure 1. A demonstration of the geometrical construction of the Fresnel zone.

P are averaged in the wavefield at **R**. This leads to the following definition of a Fresnel zone (for a plane wave):

$$x_F = (2\lambda L + \lambda^2/4)^{1/2}, \tag{1}$$

where λ is the wavelength and L the propagation distance. A phase lag of a quarter period represents the boundary between constructive and destructive interferences. However, it seems somewhat arbitrary to choose $\delta t = T/4$ as defining the region over which perturbations in phase are averaged. That is likely to depend on the nature of the measure which is drawn from seismograms. It may depend on the nature of the perturbations and the shape of the waveform.

The lack of sensitivity of waves of finite frequency to structural detail in the plane perpendicular to their path (wavefront) implies that we can think of their sampling of the medium as a volume integral within a ray tube. This tube is often assumed to take the width of the Fresnel zone (Červený & Soares 1992). Nolet (1987) defines the Fresnel zone as above (eq. 1), and a coherent arrival by $\delta t < T/4$. Yomogida (1992) suggests an efficient, approximate method of incorporating the finite volume of ray tubes into traveltime inversion. He defines the Fresnel-zone width in accordance with diffraction optics, i.e. $\delta t < T/2$. The Fréchet derivative for phase presented by Yomogida (1992) for a fixed frequency has strong side lobes, which correspond to a multitude of Fresnel zones. However, when Vasco & Majer (1993) compute the analogous quantity for a pulse of finite bandwidth the side lobes are suppressed by destructive interference. For a sufficiently broad bandwidth there will only be one Fresnel zone. This effect is demonstrated by Woodward's (1992) calculations, and by Fig. 2, which shows how the intensity of the Fresnel zones decays upon integration over frequency. This is often the case for seismic observations. A body-wave arrival recorded on a short-period instrument is generally observed as a simple pulse, not as a ringing wave train.

We have described in general terms the concepts of wavefront healing and a Fresnel zone, and pointed out the level of arbitraryness in defining the latter. The questions: (1) what is meant by 'Fresnel zone'? and (2) how should it be defined? do not have unique answers. For example, how do we choose our reference frequency when the observed wave has a significant bandwidth? In this study we set up a simple, canonical, numerical experiment to answer the latter. We use frequency–wavenumber modelling (Stolt 1978) to propagate a perturbed plane wave numerically, and estimate the effective width of the Fresnel zone for a variety of traveltime measures and waveforms. Our objective is to describe the low-pass spatial filtering effect imposed on traveltime measurements by finite frequency. We define the filter in terms of the power-spectral ratio of measured to initial phase perturbations. We explore the way in which the width of this filter varies with propagation distance and frequency.

THEORY

The equations of frequency–wavenumber migration or modelling can be found in texts on reflection seismology (e.g. Yilmaz 1987). We include a brief review for the sake of completeness. We start with the acoustic wave equation in two dimensions:

$$\left(\frac{\partial^2}{\partial x^2} + \frac{\partial^2}{\partial y^2}\right)\Phi = \frac{1}{v^2}\ddot{\Phi}, \tag{2}$$

where Φ represents the acoustic pressure, v is velocity, and $\dot{\Phi}$ is the time derivative of Φ. Fourier transforming eq. (2) in y and t (i.e. in the plane of the wavefront and in time, for a wave propagating along the x-axis) we obtain

$$\frac{\partial^2 \hat{\tilde{\Phi}}}{\partial x^2} + (\omega^2/v^2 - k^2)\hat{\tilde{\Phi}} = 0. \tag{3}$$

Here, k and ω are the transform variables for y and t, respectively. $\tilde{\Phi}(x, k, t)$ is the transform in y of $\Phi(x, y, t)$ and $\hat{\Phi}(x, y, \omega)$ is the transform in t of $\Phi(x, y, t)$. Defining the Fourier transform with a positive, complex exponent, eq. (3) has the solution

$$\hat{\tilde{\Phi}} = \hat{\tilde{\Phi}}_0 \exp(ix\sqrt{\omega^2/v^2 - k^2}) \tag{4}$$

for waves propagating forwards in the x direction. If we know the initial condition, $\hat{\tilde{\Phi}}_0$, we can compute the wavefield, $\hat{\tilde{\Phi}}$, at any propagation distance, $x = L$. We assume that the initial condition takes the form

$$\Phi_0 = \Phi(x = 0, y, t) = a(y) f(t - \delta t(y)) \Rightarrow \tag{5}$$

$$\hat{\tilde{\Phi}}_0 = \hat{f}(\omega)\mathcal{F}_y(a(y)e^{-i\omega\delta t(y)}), \tag{6}$$

where $\mathcal{F}_y(g(y))$ is the transform in y of $g(y)$. Here, $f(t)$ is a wavelet, $\delta t(y)$ a time perturbation, and $a(y)$ an amplitude modulation to what initially was a homogeneous plane wave. The wavefield at $x = L$ is

$$\hat{\tilde{\Phi}}(x = L, k, \omega) = \hat{f}(\omega)\mathcal{F}_y(a(y)e^{-i\omega\delta t(y)})\exp(iL\sqrt{\omega^2/v^2 - k^2}). \tag{7}$$

The last exponential term is a propagator which includes both translation of the field and its evolution. We can remove the translation of the field by multiplying by $\exp(-iL\omega/v)$:

$$\hat{\tilde{\Phi}}(x = L, k, \omega) = \hat{f}(\omega)e^{iL\omega/v}\mathcal{F}_y(a(y)e^{-i\omega\delta t(y)}) \times \exp[iL(\sqrt{\omega^2/v^2 - k^2} - \omega/v)]. \tag{8}$$

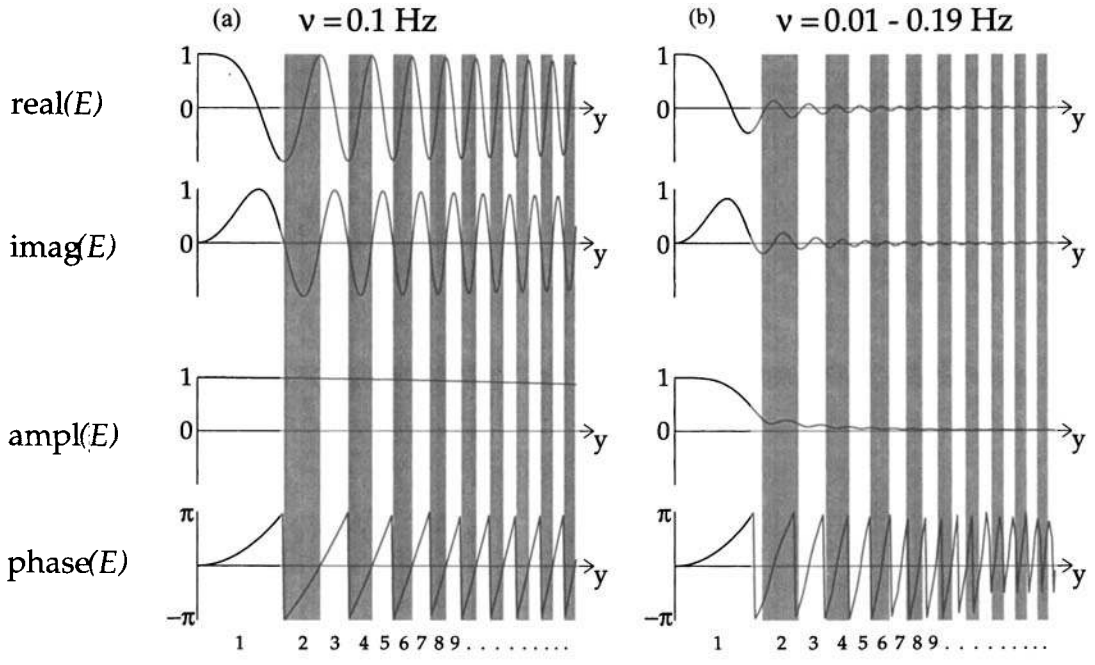

Figure 2. The real part, imaginary part, amplitude and phase of the evolutor (see eq. 10 in text) in the spatial domain. (a) The oscillations of this complex operator define the Fresnel zones for a monochromatic wave which gradually decay in amplitude and decrease in width. (b) When this operator is integrated over frequency, the side lobes, or the higher-order Fresnel zones, interfere destructively and amplitude decays quickly. If the frequency bandwidth is wide enough, one is effectively left with a single Fresnel zone.

This is the equation we solve, ignoring the translation of the wavefield. First a wavelet is specified, i.e. the function $f(t)$ is chosen. Then random time perturbations, $\delta t(y)$, are specified on the wavefront at $x = 0$, and corresponding amplitude perturbations computed according to the thin-lens approximation (Haddon & Husebye 1978), which relates amplitude perturbations to time perturbations according to

$$\delta a = \frac{-Rv}{2}\frac{\partial^2 \delta t}{\partial y^2}, \tag{9}$$

where R is the distance beyond the lens. We take R to be 100 km. The first two terms of eq. (8) can then be constructed by the Fourier transform. They are multiplied by the evolutor (propagation less translation),

$$\hat{\mathscr{E}} = \exp[iL(\sqrt{\omega^2/v^2 - k^2} - \omega/v)], \tag{10}$$

for some choice of L and the result is transformed back into the space and time domain.

The evolutor remains unchanged provided

$$L(\sqrt{\omega^2/v^2 - k^2} - \omega/v) = C = \text{constant}. \tag{11}$$

We take $C = -\pi/2$. If we rescale the wavenumber by substitution, $\sigma = 2\pi/k$, and write $\lambda = 2\pi v/\omega$ for one wavelength, then

$$L(\sqrt{1/\lambda^2 - 1/\sigma^2} - 1/\lambda) = -1/4 \Rightarrow \tag{12}$$

$$1/2\lambda L - 1/16L^2 = 1/\sigma^2. \tag{13}$$

If we assume $L \gg \lambda$, then

$$\sigma^2 = 2\lambda L + \lambda^2/4, \tag{14}$$

which defines the Fresnel zone as in eq. (1). The inverse transform in k of the above evolutor (eq. 10), i.e. $\hat{\mathscr{E}}$, describes the phase and amplitude modulation of contributions from the initial planar wavefront around **P** to the wavefield at **R** (Fig. 1) at a fixed frequency. If we assume that $a(y) = 1 + \delta a(y)$, where $\delta a \ll a$ and $\omega \delta t \ll 1$, then

$$\hat{\tilde{\Phi}}(k, \omega) = \hat{f}(\omega)\delta(k) + \hat{f}(\omega)\tilde{\delta a}(k)\hat{\mathscr{E}} - i\omega \hat{f}(\omega)\tilde{\delta t}(k)\hat{\mathscr{E}}, \tag{15}$$

where $\delta(k)$ is the delta function, and, if Φ retains the original waveform with weak perturbations in time, $\delta\tau$, and amplitude, δA, we can write

$$\tilde{\delta A}(k) = \tilde{\delta a}(k)\hat{\mathscr{E}}_{\mathrm{Re}} + \omega \tilde{\delta t}(k)\hat{\mathscr{E}}_{\mathrm{Im}}, \tag{16a}$$

$$\tilde{\delta t}(k) = \tilde{\delta t}(k)\hat{\mathscr{E}}_{\mathrm{Re}} - \frac{1}{\omega}\tilde{\delta a}(k)\hat{\mathscr{E}}_{\mathrm{Im}}. \tag{16b}$$

The Fréchet derivative of the observed time perturbation with respect to the initial time perturbation is thus the real part of the evolutor. Defining

$$\hat{\mathscr{F}}(y, \omega) = \int \hat{\mathscr{E}}_{\mathrm{Re}}(k, \omega)\mathrm{e}^{-iky}\, dk \tag{17}$$

and

$$\mathscr{F}(y) = \int_{\omega_1}^{\omega_2} \hat{\mathscr{F}}(y, \omega)\, d\omega, \tag{18}$$

the initial time perturbation maps onto the observed time perturbation via a spatial convolution with $\mathscr{F}$ for a given harmonic in the time function. If the time function has a finite bandwidth between ω_1 and ω_2, the spatial filter that acts on the initial time perturbation is $\mathscr{F}$. Note that the assumptions leading to eqs (17) and (18) are quite restrictive in that they assume no waveform distortion and no build-up of coda.

The oscillations of $\hat{\mathscr{F}}$ define the Fresnel zones for a monochromatic wave precisely (see Fig. 2a). For a finite-frequency bandwidth (Fig. 2b), the side lobes are attenuated and the first

Fresnel zone narrows. For a sufficiently wide frequency band we are left with a single Fresnel zone.

It is tempting to continue this analysis and insert eq. (9) into eq. (16b). Bear in mind that the assumptions made prior to eq. (16) are restrictive; they will generally not hold in the Earth or in feasible numerical experiments except at very long periods. But, if we do, we obtain

$$\tilde{\delta\tau}(k) = \tilde{\delta t}(k)\left(\hat{\mathscr{E}}_{\mathrm{Re}} - \frac{Rv}{2\omega}k^2\hat{\mathscr{E}}_{\mathrm{Im}}\right). \tag{19}$$

The quantity

$$\tilde{\mathscr{G}}(k) = \int_{\omega_1}^{\omega_2}\left(\hat{\mathscr{E}}_{\mathrm{Re}} - \frac{Rv}{2\omega}k^2\hat{\mathscr{E}}_{\mathrm{Im}}\right)d\omega \tag{20}$$

is the spatial transfer function for the traveltime perturbation. We plot $\tilde{\mathscr{G}}^2$ in Fig. 3 for a monochromatic wave, for a wave of narrow bandwidth, and for a wave of wide bandwidth. The bandwidths are chosen to be roughly equivalent to the numerical examples presented later. The transfer function for the narrow-band wave has a few significant side lobes, while for the broadband wave it has none. The first side lobe occurs at a wavenumber which is roughly double the width of the central peak in the transfer function. Contributions to time perturbations from initial perturbations of amplitude are small for the parameters used here (compare solid and dashed lines in Fig. 3).

METHOD

We start with a simple plane wave. Complexity is introduced to the plane wave by the thin-lens approximation as it passes through a hypothetical lens of heterogeneity. We then follow the evolution of the introduced complexity as the perturbed wavefield advances through a homogeneous medium using frequency–wavenumber modelling (see Fig. 4). In reality, the Earth does not offer this situation. In the Earth, heterogeneity persists throughout a finite volume, and complexity is continually inserted into a wavefield that traverses it. At the same time, the previously introduced complexity continues to evolve. In order to estimate diffraction effects on traveltime measurements at a given, fixed propagation distance we idealize the situation in this manner. Having propagated the wavefield a given distance we measure the traveltime from densely spaced seismograms and compare the detailed spatial variation of the measured traveltime with the initial phase perturbations. Of course, if we measured the full wavefield we could migrate it back to the initial condition and thus recover all of its detail. However, in earthquake seismology we generally have sparse recordings of the wavefield and extract only a very simple measure from the seismogram, traveltime or some norm of a misfit of a waveform to a synthetic waveform. Such sparse and simple measures do not allow us to recover all the detail of the initial condition.

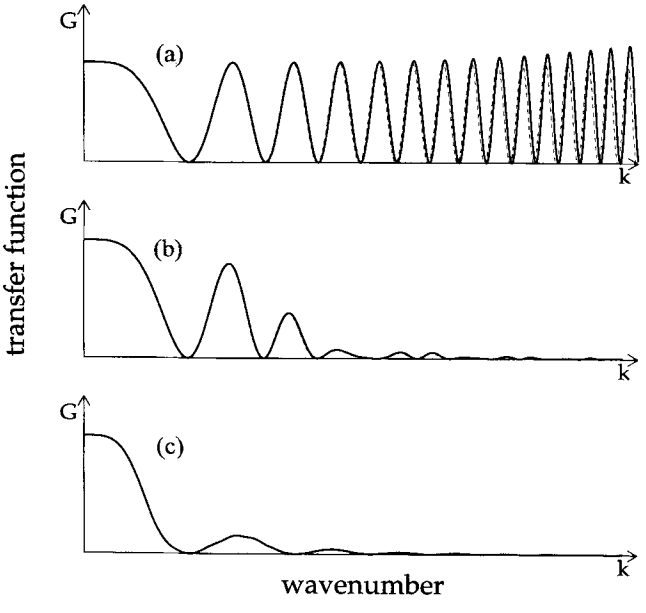

Figure 3. The theoretical transfer function for phase according to eq. (20). The centre period is the same in all cases. (a) monochromatic; (b) with spectral bandwidth equal to half the centre frequency; (c) with spectral bandwidth equal to one-and-a-half times the centre frequency. The dashed curve ignores the second term of eq. (20), which is due to initial perturbations in amplitude. It is indistinguishable from the solid curve in (b) and (c).

Calculations were done with 8192 time steps and a time resolution of 0.02 s. The wavefront was sampled 512 times at a space of 5 km. The propagation velocity was 10 km s^{-1}. The initial wavelet was chosen as a Gaussian, $f(t) = \exp(-t^2)$, and shifted 50 s into the 164-s long time window. It has significant energy for frequencies up to $1/\pi$ Hz. The phase perturbation, δt, is randomly generated with a Gaussian power spectrum of variable width of the order of tens of kilometres. At least 10 spatial samples fall within one correlation length of the time perturbation and a wavelength is comparable in size or larger. The time perturbation is given a root-mean-square (rms) value of 1/2 s. This choice of parameters ensures that time can be measured accurately enough and with sufficient spatial and spectral resolution.

Fig. 4 shows an example where an initial condition has been propagated to progressively greater distances. Each frame shows a record section with time progressing downwards and distance along the wavefront going across the sheet. Alternatively, we can regard each frame as representing a snapshot of a wavefield propagating up the page. The dark, large-amplitude portion of the field is the wavefront. Initially it contains considerable complexity. As the wave propagates further the wavefront becomes smoother, the initial pulse becomes broader, the diffraction hyperbolae become wider, and the coda tail extends further behind the wavefront. At each propagation distance we can measure the arrival time from each spatial sample of the wavefield, i.e. the 512 seismograms. Thus, we sample an empirical function $\delta t(y)$ discretely. The power spectrum of this function, $P_{\delta\tau} = |\tilde{\delta\tau}(k)|^2$ provides information on the smoothness of the function, and the ratio of the power, $P_{\delta\tau}$, to the power of the initial condition, $P_{\delta t} = |\tilde{\delta\tau}(k)|^2$, describes what effect propagation has had on the observed traveltime variations. We propagate a number of independently generated initial conditions to a set of fixed distances, measure time, $\delta\tau$, and construct the power-spectral ratio, $S(k) = P_{\delta\tau}/P_{\delta t}$. The ensemble average of 10–20 randomly realized spectral ratios then defines an empirical measure of the spatial filtering effect of propagation.

Frequency is also expected to affect the degree of smoothing. In order to measure the effect of frequency we defined five narrow frequency bands within the bandwidth of the initial

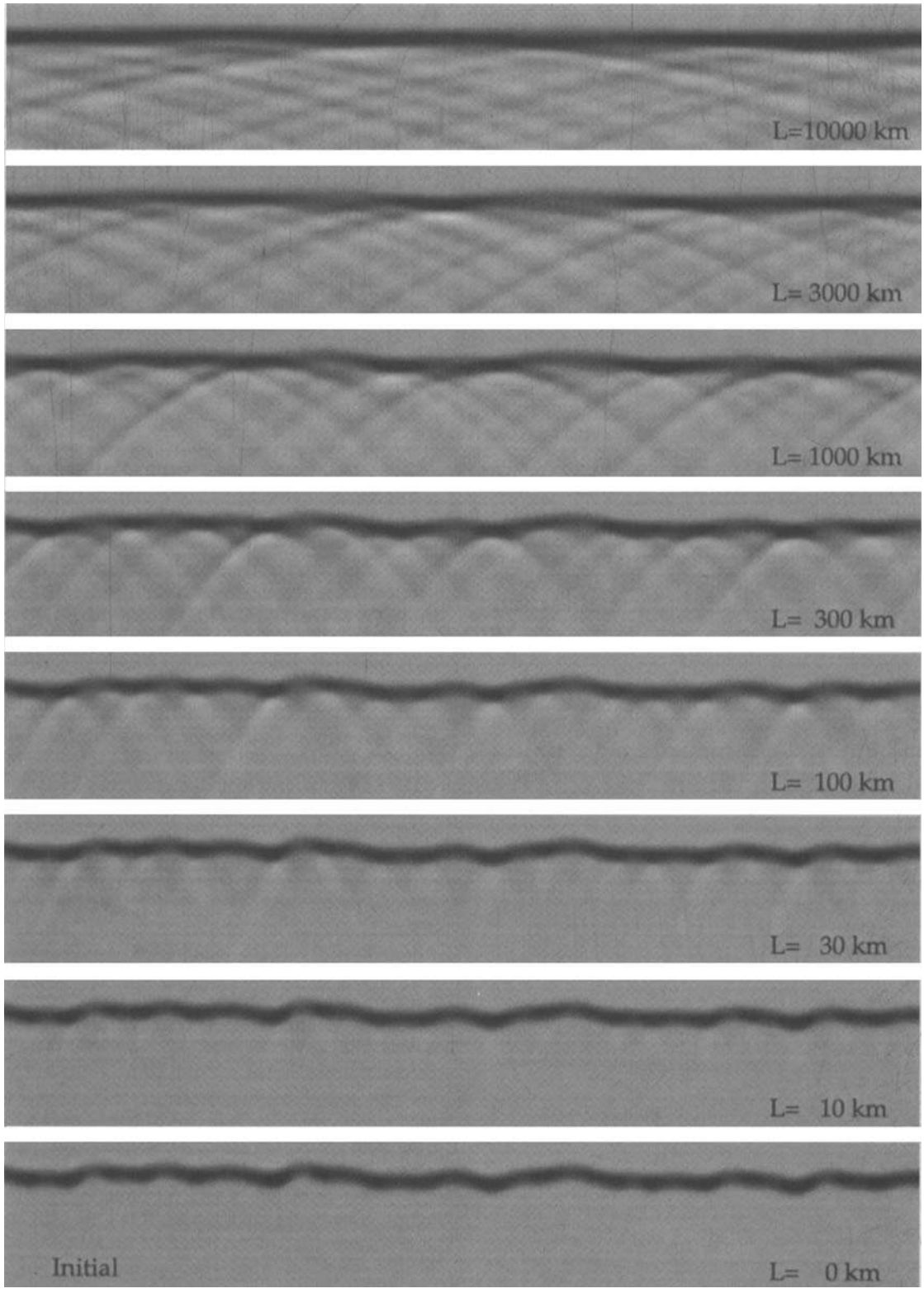

Figure 4. The evolution of complexity in a propagating plane wave. Each frame represents a record section. Time progresses downwards, distance along the wavefront goes across the page. The length of the time window is 20.48 s. The length of the section is 2560 km. Propagation distance progresses from $L = 0$ to 10 000 km.

time function, $f(t)$. Since the observed field is linear in $f(t)$ we convolve the propagated field with a filter corresponding to each frequency band. Traveltime is measured and an ensemble average of a power-spectral ratio is constructed as before, for a fixed propagation distance, chosen as $L = 1000$ km. The filters are Gaussian in shape, and either zero-phase (acausal) or minimum-phase (causal).

A number of techniques are used in seismology to measure

traveltime. Sometimes traveltime is measured by correlating an observed waveform and a synthetic waveform (e.g. Su & Dziewonski 1992). The peak of that correlation defines the traveltime. Time is often measured off a graph by visual inspection. This involves visual pattern recognition based on experience, and incorporates changes in amplitude and frequency on a trace. This process cannot be defined analytically. We try as our measures of traveltime a range of methods: (1) automated picking where the amplitude has reached 1/8 of the peak amplitude; (2) automated picking at the first amplitude maximum; (3) picking by correlation over a time window which spans 3, 5, 7 periods, or the whole trace.

RESULTS

Our objective is to describe empirically the low-pass spatial filtering effect imposed on traveltime measurements, which we define in terms of the power-spectral ratio of measured to initial time perturbations. We seek to explore the way in which the width of this filter varies with propagation distance and frequency, and to calibrate it in absolute terms. We turn our focus first to the effect of propagation distance. Fig. 5 shows the ensemble-average of spectral ratios for seven propagation distances spanning three orders of magnitude. In this instance, the broad-band wavelet, $f(t) = \exp(-t^2)$, was used unfiltered and the measurement was done by automated picking where 1/8th of the peak amplitude was reached. The symbols represent the empirically determined spectra (by the procedures described earlier) and are defined in the legend. The curves represent parametric fits to the empirical spectra given two degrees of freedom.

$$S(k) = \frac{1}{1 + (kx_c/2\pi)^n}, \tag{21}$$

where k is the wavenumber, x_c is a free parameter which describes the width of each curve, and n is a free parameter which describes the rate of decay of each curve. We have no theoretical justification for this particular choice of curve; however, this analytical form fits the data well. The spectra in Fig. 5 are simple, have no side lobes, and are similar in shape to those in Fig. 3(c). The spectral ratios narrow regularly as propagation distance increases. This is expected (the Fresnel zone widens with increasing distance). The critical scale, x_c, is defined by $x_c = 2\pi/k_c$, where k_c is the wavenumber where each curve has decayed to a value of 1/2. x_c is a measure of the width of the spectral peak. Note that the level of the spectral ratio tends stably to unity at small wavenumbers. This means that no amplification or attenuation of large-scale features occurs during propagation. The experiment was repeated using different measures of traveltime. Both cross-correlation of waveforms and picking at maximum amplitude were considered and yielded indistinguishable spectral shapes. We expect the average time of the measured wavefront $\overline{\delta\tau}$ to become slightly negative as propagation distance increases. Advanced portions of the wavefront spread and mask the delayed parts. We do observe this effect (see Table 1), but do not focus on it further. The parametric fits of Fig. 5 and the average time of the front, $\overline{\delta\tau}$, are listed in Table 1. The exponent,

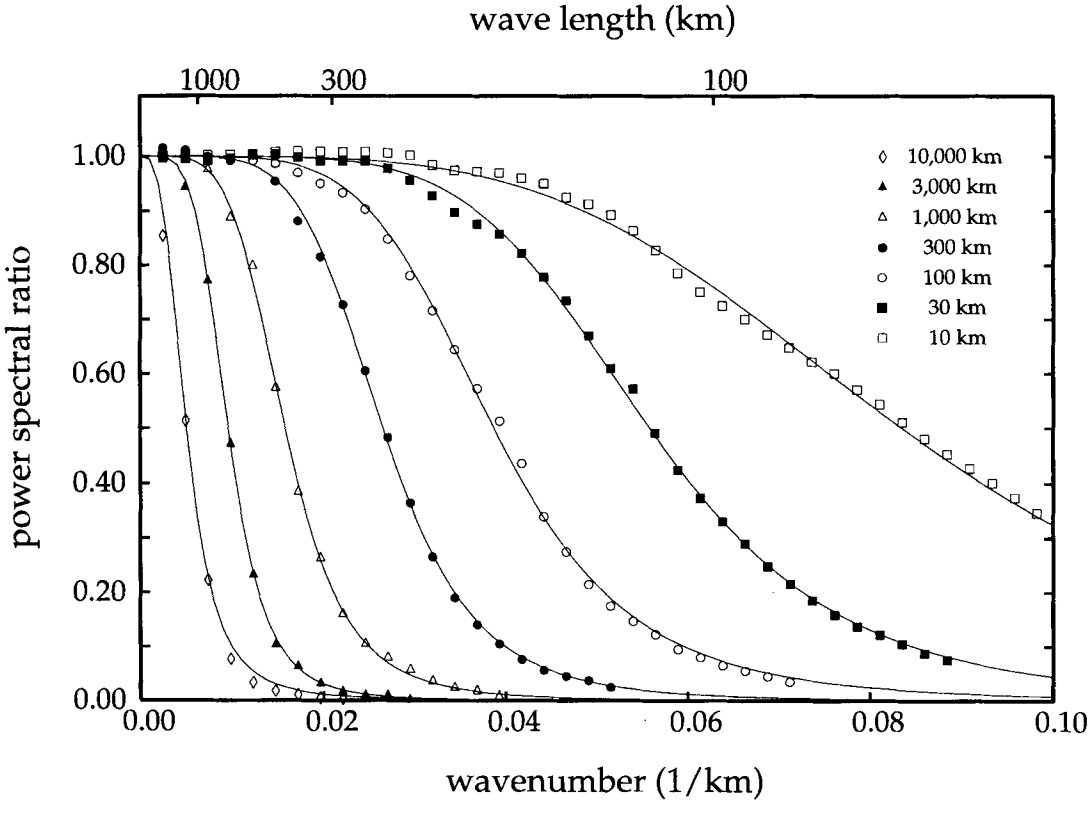

Figure 5. Power-spectral ratios of traveltime measurements and the initial traveltime perturbation for varied propagation distance. Measurements were made by picking from broad-band seismograms. This ratio is indictive of the width of the spatial filtering imposed by propagation effects.

Table 1. Results of parametric fits to data in Fig. 4.

L (km)	x_c (km)	n	$\overline{\delta\tau}$ (seconds)
10	63.8	4.0	-0.003
30	91.7	4.6	-0.008
100	130.5	4.8	-0.021
300	199.1	4.3	-0.047
1,000	332.5	4.9	-0.083
3,000	575.4	4.3	-0.111
10,000	1029.9	4.0	-0.131

n, varies little with propagation distance. Its average value is 4.4. Thus the shape of the filter is approximately described by a second-order Butterworth function. The average time shift, $\overline{\delta\tau}$, also increases regularly with increasing distance, L. This increase is much slower than linear in L. Consequently, the deviation of apparent velocity from true velocity tends to zero with increasing distance. This means that the velocity shift caused by diffraction, which is associated with wavefront healing, does not affect the asymptotic level of the apparent velocity shift due to ray-bending effects, which was described by Roth *et al.* (1993). The quantity in Table 1 that is of most interest is the critical scale, x_c. It increases regularly with distance and is determined with an uncertainty of the order of 5 per cent based on the least-squares misfit. This relationship is plotted in Fig. 6(a). It is fit by the Fresnel-zone formula in eq. (1) with the wavelength chosen as $\lambda = 80$ km, which corresponds to a period of $T = 8$ s. It is clear that the functional behaviour of $x_c(L)$ is matched by the Fresnel-zone formula. However, the choice of reference frequency or period is somewhat arbitrary for this broad-band wavelet.

The frequency bands used to map the frequency dependence of x_c are centred on periods of $T_c = 3.40$, 5.24, 8.67, 15.71 and 26.18 s. Their spectra are Gaussian. The bandwidth is proportional to the centre frequency, and the filters overlap at the point where the amplitude spectra take a value of 1/e. The phase spectra of the filters were not found to affect relative time measurements. Occasional problems with cycle skipping were encountered in the highest frequency bands, where the period is comparable to the maximum time perturbation. The length of the time window over which correlation was computed had no effect. Correlations with the unperturbed time function convolved with the same filter as the propagated wavefield, and computed over time windows of length $3T_c$, $5T_c$, $7T_c$, or the whole trace, all peak at essentially the same time. However, we found a difference between traveltime measurements made by onset picking and by waveform correlation. The spectral ratios for the five frequency bands and automated picking are shown in Fig. 7. The equivalent results of correlation measurements of traveltime are also shown in Fig. 7. In both cases, stable estimates of the spectral ratio are achieved which tend to unity at small wavenumbers. The width of the spectral peak at low wavenumbers decreases regularly with increasing period. Here we observe a clear side lobe to the spectral peak at low wavenumbers. The centre wavenumber of this secondary spectral peak scales roughly with the width of the primary spectral peak. In this case, we fit a function of

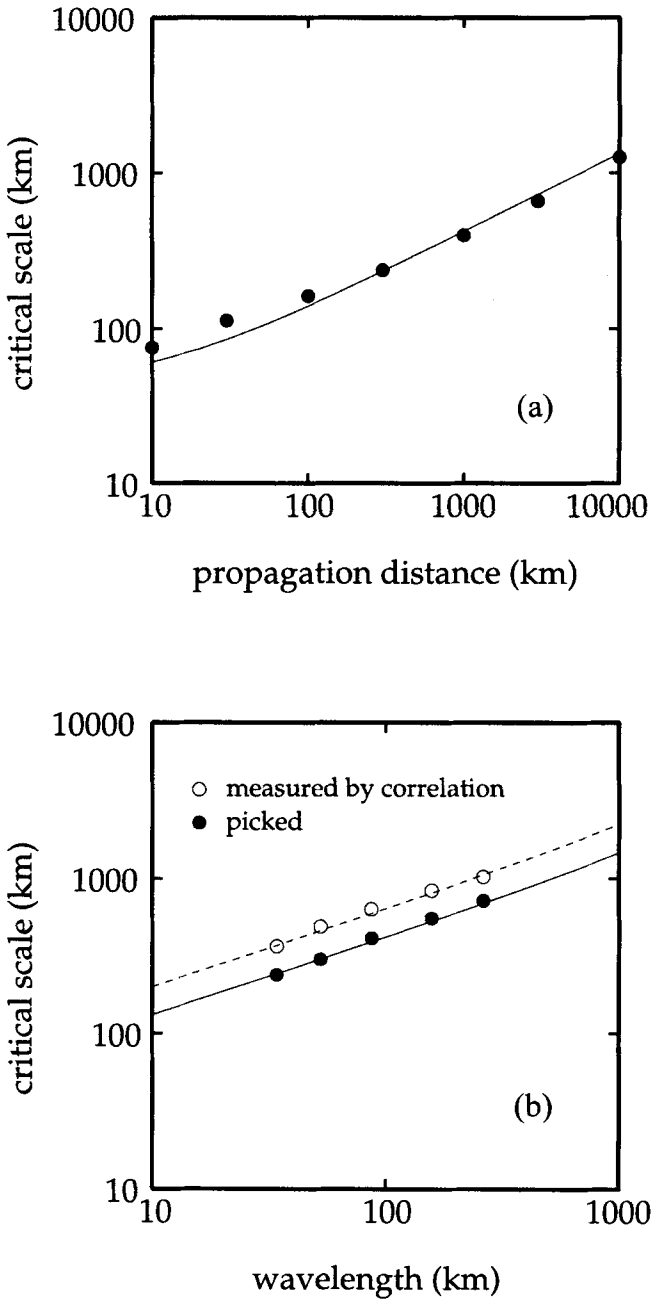

Figure 6. The empirically determined dependence of the scale of smoothing on propagation distance and wavelength (λ). The curves correspond to Fresnel formulas such as eq. (1).

the form

$$S(k) = \frac{1}{1+(kx_c/2\pi)^n} + \frac{A(kx_b/2\pi)^l}{[1+(kx_b/2\pi)^m][1+(kx_b/2\pi)^l]}, \qquad (22)$$

where k is the wavenumber as before, but there are now six free parameters, i.e. the scales x_c and x_b, the exponents n, m and l, and the amplitude of the secondary peak, A. Again we have no justification for this analytical form other than that data are reasonably well fit. Consequently, we cannot attach any significance to the above parameters other than the two scales. The results of the parameter fit are presented in Table 2. The exponents, n, m, and l, are now less uniform than before

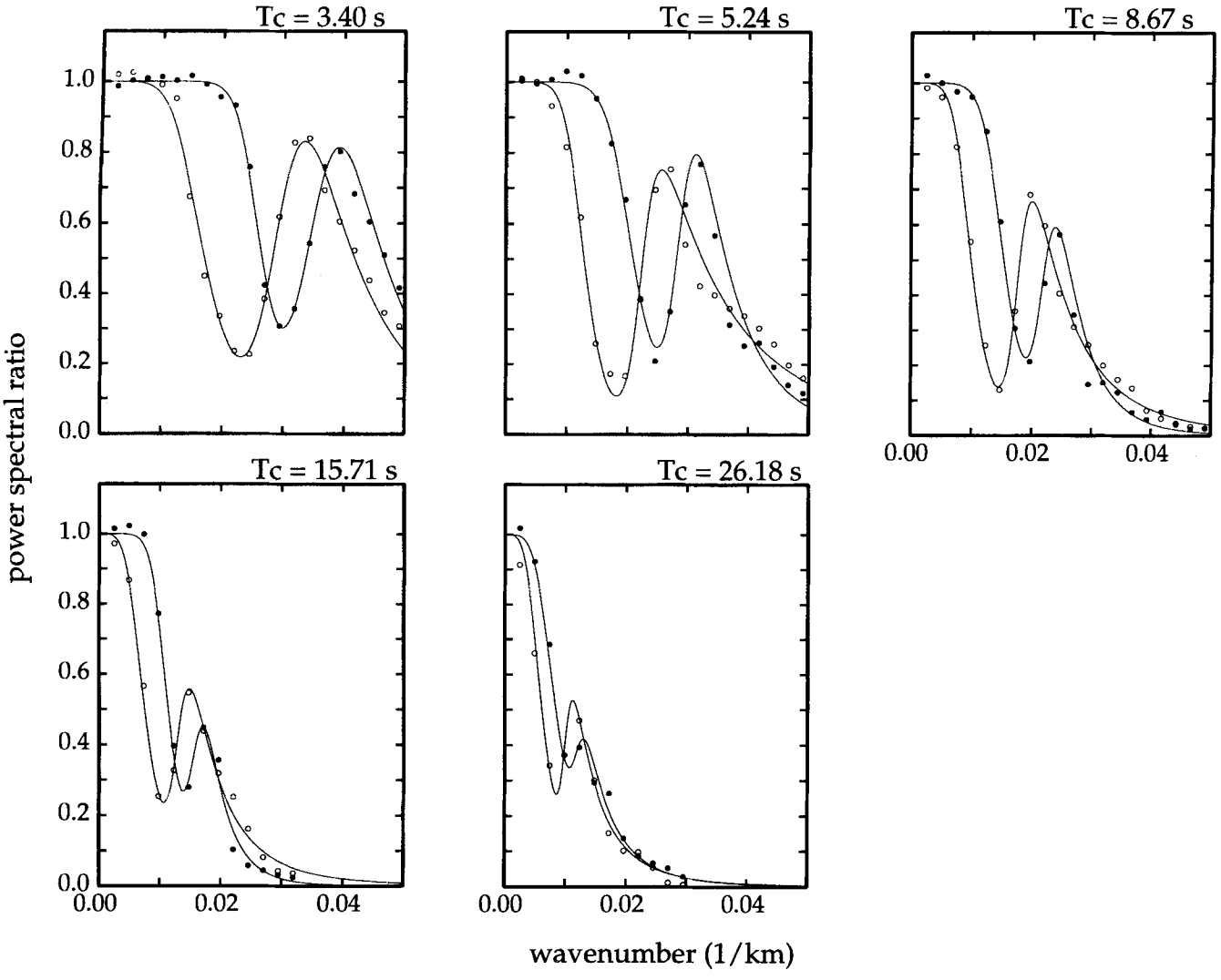

Figure 7. As Fig. 4, except here measurements were done at a fixed propagation distance of 1000 km but from narrow-band filtered seismograms of varied frequency, by onset picking (solid circles), and by waveform correlation (open circles).

Table 2. Results of parametric fits to data in Figs 5 and 6. (a) Picking measurements; (b) correlation measurements.

(a)

T_c (sec)	x_c (km)	n	A	x_b (km)	m	l
3.4	239	13.5	3.0	170	6.6	12.7
5.2	301	8.7	2.5	215	6.3	20.0
8.7	412	7.7	1.9	279	7.0	18.0
15.7	554	7.8	1.4	388	6.9	15.1
26.2	723	4.3	0.9	520	4.1	14.9

(b)

T_c (sec)	x_c (km)	n	A	x_b (km)	m	l
3.4	366	5.9	2.8	204	4.9	11.9
5.2	490	7.1	2.1	276	3.3	16.9
8.7	635	5.7	1.9	348	4.1	16.5
15.7	837	4.3	1.6	468	4.0	12.9
26.2	1024	4.0	1.3	618	3.7	15.9

because they are not determined as well since more degrees of freedom are allowed in the fit. The scales, x_c and x_b, increase regularly with increasing period. They are determined with an uncertainty of the order of 5 per cent on the least squares misfit of the curve fitting. x_c in eq. (22) corresponds to x_c in eq. (21), and represents a scale which is the inverse width of the primary spectral peak at low wavenumbers. x_b does not represent the position of the secondary peak. From the data in Fig. 7 for picked times we find that the secondary spectral peak occurs near $k = 2k_c (k_c = 2\pi/x_c)$. From the data in Fig. 7 for correlation measurements we find that the secondary peak occurs at about $k = 1.5k_c$. Again, however, the parameter of most importance to us is x_c, together with its relation to frequency or period. This relationship is plotted in Fig. 6(b) for both picked and correlated time measurements. For reference we show two Fresnel-zone formulas, one defined by a time delay of a quarter period (solid), and another defined by a time delay of half a period (broken). The reference period is chosen as the centre period, T_c, of each narrow-band filter. It is clear that the frequency dependence of the critical scale is well fit by a Fresnel-zone formula. It is also clear that the Fresnel zone for correlated traveltimes is wider than the Fresnel zone for picked traveltimes. The Fresnel zone for the former is calibrated as the Fresnel zone of diffraction optics, according to a time delay of half a period. For the latter the Fresnel zone is calibrated as defined by a time delay of a quarter of one period.

DISCUSSION

Some of the features of Figs 5–7 deserve further discussion. We concentrate first on the simple form of the spectral ratios in Fig. 5. Here the wavelet is broad band ($\nu < 1/\pi$) and the spectral ratios have no side lobes. We suggest that this may be explained by the simple effect demonstrated in Figs 2 and 3. Because of the broad-band nature of the waveform, the higher-order Fresnel zones interfere destructively and we are left with only one Fresnel zone. The spectral ratios look very similar to the transfer function in Fig. 3(c). In Fig. 7 we observe clear side lobes in the spectra. Here, the relevant comparison is to Fig. 3(b), which has a few significant side lobes present. The relative position of the side lobes in Fig. 7 to the width of the central peak matches roughly the structure of the transfer function in Fig. 3 (it occurs at about $k = 2k_c$).

We have looked in further detail at contributions to measured traveltimes from the secondary spectral peak. We filtered both the initial time perturbation and the measured time delay spatially, by filters corresponding to the spectral shapes under each of the primary and secondary spectral peaks. We found that the contributions from the primary spectral peak correlate at a level of 0.9 to 0.95. We can therefore claim that that component of spatial variability in the time measurements is a local average of the initial time perturbation. On the other hand, contributions from the secondary spectral peak have a correlation coefficient of 0.0 to -0.2. This component of the spatial variability of the time measurement therefore represents noise. It is not a local average of the initial time perturbation as one would expect if the arguments leading to eq. (20) were valid. It is evident from Fig. 8 that small-scale features of the time measurement (trace labelled 'measured') do not correlate with the small-scale features of the initial time perturbation (trace labelled 'initial'). This noise is present in both picked times and times measured by correlation. We therefore suggest that it has to do with the structure of the wavefield adjacent to the wavefront. It is a non-linear effect, not described by the linearized eq. (20). We suggest that it is related to the complex interference patterns that occur in part in front of the main arrival where it is delayed.

The difference in the Fresnel-zone scaling between picked traveltimes and traveltimes measured by correlation is intriguing. It is clear that the former measurement concentrates on the onset of the waveform, while the latter incorporates the whole of the waveform. We can therefore argue that the latter includes effects that are further delayed in time behind the initial wavefront, such as diffraction hyperbolae due to features in the initial wavefront farther afield from the direct path. Thus we argue that we can explain qualitatively why picked traveltimes offer better spatial resolution than traveltimes measured by correlation, while we cannot quantitatively explain the differences we observe in Fig. 6(b).

Neither the component of small-scale noise nor the dependence of the effective Fresnel-zone width on the type of measure of time are predicted by linearized theory, which does not incorporate the type of measure explicitly. We must thus ask if the non-linear effects present in the simulations are realistic. We take an example from teleseismic body waves. If the lower mantle contains velocity heterogeneity of the order of a fraction of a per cent on a scale of 1000 km, as Gudmundsson, Davies & Clayton (1990) suggest, then we expect time fluctuations originating in the lower mantle of the order of 0.1 s (rms). With recording at frequencies lower than 1 Hz, the condition $\omega \delta t \ll 1$ is not met like in the experiments presented here. We therefore argue that the design of the experiments is relevant to real problems.

It is sometimes argued that if diffraction or scattering effects are significant in a wavefield then they can be recognized in the waveform of a single observation. The recognizable aspects of the waveform would be pulse broadening and an emergent onset of the waveform. We argue on the basis of the numerical experiments presented here that in a ringing, narrow-band seismogram this is not the case. Waveform distortion may be minor and undetectable in a single seismogram, while diffraction effects on timing are significant. Fig. 8 shows an example of how waveforms are distorted due to interference of diffraction effects. The top trace shows an unperturbed waveform, narrow-band filtered. The section below shows perturbed waveforms convolved with the same filter. Every fifth calculated trace is displayed. Individual seismograms do not differ much from the top trace, although we can recognize distortion in the section. Much healing has already taken place ($L = 1000$ km). Note the small-scale features of the measured traveltimes which do not correlate with small-scale features of the initial condition. Despite a measurement of traveltime from noise-free seismograms, here by a correlation technique, considerable uncertainty is injected into the time measurement.

CONCLUSIONS

Seismic tomography uses time information contained in seismograms in order to map the internal structure of the Earth in terms of variable wave speed. When body waves are used, the data are traveltimes. When surface waves are used, the data are dispersion curves, or phase velocity as a function of frequency. In both cases a common assumption is that of ray

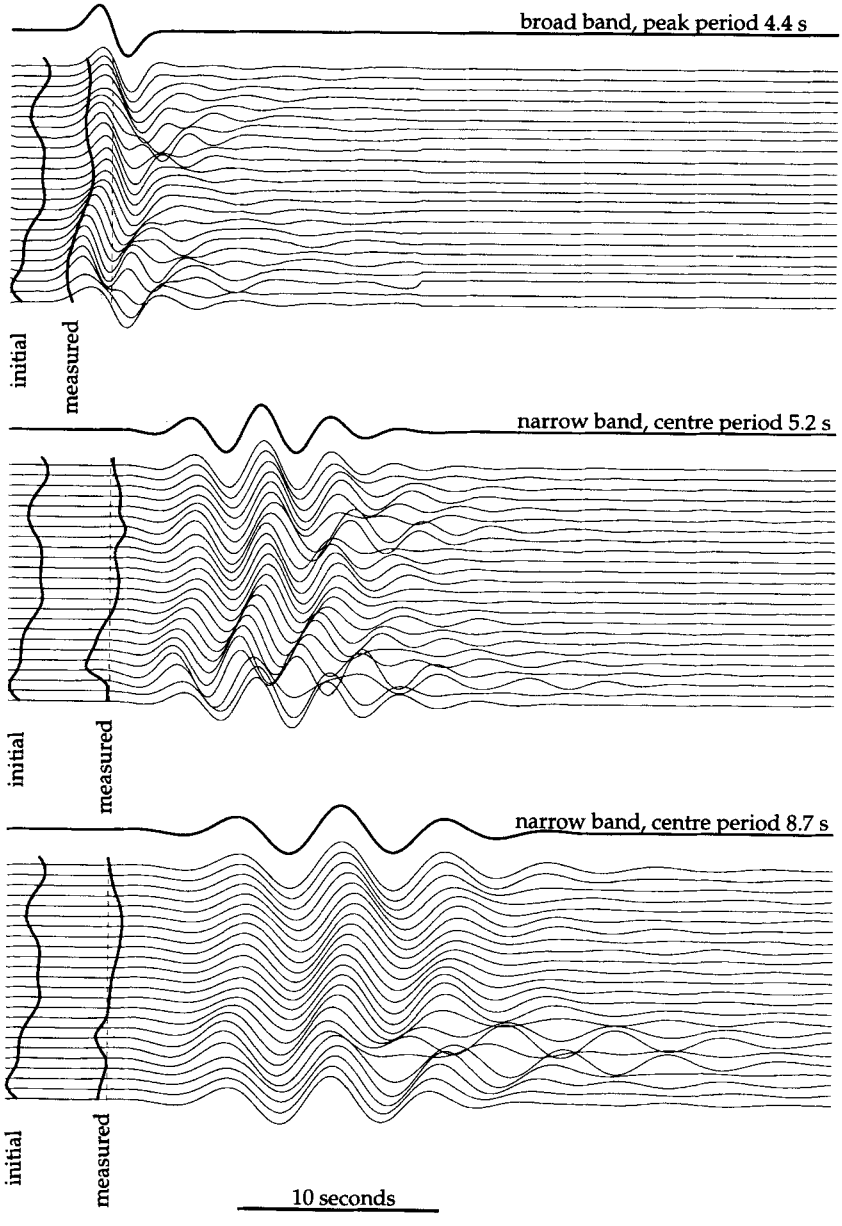

Figure 8. Waveform distortion due to interference of diffraction effects or scattering. The top trace in each of three cases shows an unperturbed waveform, narrow-band filtered. The section below shows perturbed propagated waveforms convolved with the same filter. Every fifth calculated trace is displayed.

theory. Body-wave energy is assumed to travel along infinitesimally thin rays. Surface waves are assumed to travel along great-circle paths. When the resolution of seismic tomography is appraised, the same assumptions are made. The resolution estimate is based on the ray approximation and incorporates only the density of paths as described by rays. However, in practice all observed waves sense a finite volume of the medium. Wavefront healing imposes a low-pass spatial filter on the resolution of phase measurements. The shape of this filter is empirically described by a second-order Butterworth function and therefore has a sharp cut-off in wavenumber or scale. The variation of the width of the spatial filter with propagation distance and frequency is described by the Fresnel zone. Note that these numerical results apply to a regime where the initial time perturbation cannot be written as a linearized perturbation term, a case often encountered in seismology. For traveltimes measured by onset picking, the Fresnel zone is defined by a time delay of $|\delta t| < T/4$ (here T is one period). The width of the Fresnel zone for traveltimes measured by correlation is wider, defined by a time delay of $|\delta t| < T/2$. For narrow-band waveforms, measured time includes small-scale contributions that are not local averages of the initial time perturbation and thus represent noise.

ACKNOWLEDGMENTS

We thank Tod Nestor, Malcolm Sambridge, Phil Cummins and Brian Kennett for helpful discussions on the subject of this study. Malcolm Sambridge read an early version of the manuscript critically and greatly improved its presentation.

We are indebted to an anonymous reviewer whose critique led us to clarify the manuscript.

REFERENCES

Červený, V. & Soares, J.E.P., 1992. Fresnel volume ray tracing, *Geophysics,* **57,** 902–15.

Claerbout, J.F., 1976. *Fundamentals of Geophysical Data Processing, Blackwell, Oxford.*

Claerbout, J.F., 1985. Imaging the Earth's Interior, Blackwell, Oxford.

Gudmundsson, O., Davies, J.H. & Clayton, R.W., 1990. Stochastic analysis of global traveltime data: mantle heterogeneity and random errors in the ISC data, Geophys. J. Int., **102,** 25–44.

Haddon, R.A.W. & Husebye, E.S., 1978. Joint interpretation of P-wave time and amplitude anomalies in terms of lithospheric heterogeneities, *Geophys. J. R. astr. Soc.,* **55,** 19–43.

Nolet, G., 1987. Seismic wave propagation and seismic tomography, in *Seismic Tomography,* pp. 1–23, ed. Nolet, G., D. Reidel, Dordrecht.

Nolet, G. & Moser, T.-J., 1993. Teleseismic delay times in a 3-D Earth and a new look at the *S* discrepancy, *Geophys. J. Int.,* **114,** 185–195.

Petersen, N.V., 1990. Inverse kinematic problem for a random medium in geometric optics approximation, *Pageoph.,* **132,** 417–437.

Roth, M., Muller, G. & Snieder, R., 1993. Velocity shift in random media, *Geophys. J. Int.,* **115,** 552–563.

Sambridge, M. & Snieder, R., 1993. Applicability of ray-perturbation theory to mantle tomography, *Geophys. Res. Lett.,* **20,** 73–76.

Stolt, R.H., 1978. Migration by Fourier transform, *Geophysics,* **43,** 23–48.

Su, W-j. & Dziewonski, A.M., 1992. On the scale of mantle heterogeneity, *Phys. Earth planet. Inter.,* **74,** 29–54.

Vasco, D.W. & Majer, E.L., 1993. Wavepath traveltime tomography, *Geophys. J. Int.,* **115;** 1055–1069.

Wielandt, E., 1987. On the validity of the ray approximation for interpreting delay times, in *Seismic Tomography,* pp. 85–98, ed. Nolet, G., D. Reidel, Dordrecht.

Woodward, M.J., 1992. Wave-equation tomography, *Geophysics,* **57,** 15–26.

Yilmaz, O., 1988. *Seismic Data Processing,* Soc. Explor. Geophys., Tulsa, OK.

Yomogida, K., 1992. Fresnel-zone inversion for lateral heterogeneities in the Earth, *Pageoph.,* **138,** 391–406.